RAA 2017 Vol. **17** No. **1**, 2 (10pp) doi: 10.1088/1674–4527/17/1/2

http://www.raa-journal.org *http://iopscience.iop.org/raa*

***R**esearch in*
***A**stronomy and*
***A**strophysics*

Extension of the rotating dipole model with oblateness of both primaries

Xiang-Yuan Zeng[1]⋆, Xiang-Dong Liu[1] and Jun-Feng Li[2]

[1]School of Automation, Beijing Institute of Technology, Beijing 100081, China; *zeng@bit.edu.cn*
[2]School of Aerospace Engineering, Tsinghua University, Beijing 100084, China; *lijunf@tsinghua.edu.cn*

Received 2016 May 29; accepted 2016 September 9

Abstract A rotating mass dipole can be used to understand the dynamical behaviors around elongated asteroids as well as binary asteroids. In this paper an improved dipole model with oblateness in both primaries is investigated. The dynamical equations of a particle around the improved model are first derived by introducing the oblateness coefficients. The characteristic equations of equilibrium points are obtained, resulting in the emergence of new equilibria in the equatorial plane and the plane xoz depending on the shape of the spheroid. Numerical simulations are performed to illustrate the distribution of these equilibrium points. Significant influence from the oblateness of the primaries on the topological structure is also analyzed via zero-velocity curves.

Key words: celestial mechanics — minor planets, asteroids: general — methods: numerical

1 INTRODUCTION

The scientific exploration of asteroids and comets has again come into focus after the successful flight of the ROSETTA mission along with the groundbreaking soft landing of the Philae probe on the comet 67P/Churyumov-Gerasimenko. The mission, proposed and performed by ESA, aimed to gain a better understanding of comets as well as the early solar system[1]. In fact, there have been several missions involving minor bodies over the past decades, with targets ranging from near Earth asteroids to the Kuiper belt. For example, the Hayabusa spacecraft, developed by JAXA, performed the first sample return mission from an asteroid, 25143 Itokawa, during a seven year mission (Tsuchiyama et al. 2011). The more recent New Horizons, launched by NASA in 2006, successfully made a flyby of the dwarf planet Pluto on 2015 July 14 and also aims to have a flyby encounter with one or two Kuiper belt objects (Fountain et al. 2008). In addition, an ambitious future space mission proposed by NASA was funded in March 2015, and is known as the Asteroid Redirect Mission (ARM). The spacecraft will rendezvous with a near Earth asteroid and may transport a boulder from its surface to a stable lunar orbit[2].

Besides the above practical achievements, a lot of theoretical progress has also been made, including but not limited to trajectory design (Gong et al. 2009; Zou et al. 2014), the dynamical model for asteroids (Scheeres 2014) and some innovative orbiting methods (Zeng et al. 2015b, 2016b). Regarding those fundamental problems, one big challenge is to construct the gravitational model for an irregularly shaped central body. Due to various irregular shapes of minor bodies, the widely used spherical harmonic model cannot be simply applied to those bodies where the function would converge very slowly or even diverge near the body's surface (Cui & Qiao 2014). In order to overcome this problem, a new method, i.e., the polyhedral model, was proposed by Werner & Scheeres (1996) and applied to the asteroid 4769 Castalia. Due to the high accuracy of this model based on the geometrical shape of the central body, it has been widely employed in numerous studies to obtain the precise gravitational field, including the asteroid 4179 Toutatis (Scheeres et al. 1998), Eros (Yang et al. 2015), Itokawa, 216 Kleopatra, (8567) 1996 HW1 (Wang et al. 2014) and so on. Through observation, it can be easily found that the aforementioned asteroids maintain an elongated shape even with different sizes. Some of them can also be

⋆ Partially presented at the 2015 AAS/AIAA Astrodynamics Specialist Conference, Vail, CO, August 9-13, 2015

[1] *http://www.esa.int/Our_Activities/Space_Science/Rosetta*

[2] *http://en.wikipedia.org/wiki/Asteroid_Redirect_Mission*

referred to as contact binary asteroids (Magri et al. 2011) or dumbbell-shaped bodies. In particular, the successful flyby of Toutatis by the Chinese Chang'e-2 spacecraft (Huang et al. 2013) has brought us many new insights (Zhao et al. 2015; Jiang et al. 2015) into this near-Earth asteroid.

As typical irregularly shaped bodies, elongated asteroids or comets have been the target of a considerable number of investigations. Some alternative methods are also presented to better understand the dynamics near those elongated bodies, such as a rotating mass dipole (Goździewski 1998), a massive straight segment (Elipe & Lara 2003), perpendicular material segments (Bartczak & Breiter 2003) or a simple dumbbell-shaped body consisting of two spheres and a cylinder (Li et al. 2013). These studies usually focus on the dynamics around these simple models, rather than the connection between these models and the minor bodies. An attempt from Elipe & Lara (2003) has been made by using a finite straight segment to approximate the exterior potential of asteroid Eros. Another earlier investigation was conducted by Prieto-Llanos & Gomez-Tierno (1994) who adopted the rotating mass dipole to approximate the Mars-Phobos system.

Recently, Zeng et al. (2015a) proposed a method to approximate the potential distribution outside of natural elongated bodies by using the rotating mass dipole in which several sample minor bodies were illustrated. The essence of this method is to make the equilibrium points of the dipole model coincide with the central body as much as possible through adjusting the associated system parameters. The dipole model was proposed by Chermnykh in 1987 (Chermnykh 1987), which was adopted to approximate the gravitational field of a dumbbell (Kokoriev & Kirpichnikov 1988). As is known in this field, the polyhedral method can give an accurate potential distribution, but it needs to discretize the geometrical surface of each target body. However for the rotating dipole model, this approach may provide some common characteristics of elongated celestial bodies by only varying its system parameters.

The equilibrium points of irregularly shaped asteroids are always a key point in understanding the dynamical behaviors around these bodies (Ostro et al. 2000). Mondelo et al. (2010) presented the four equilibrium points around 4 Vesta along with their stabilites. By using the polyhedral method, Wang et al. (2014) investigated the location and stability of equilibrium points of 23 minor bodies, including asteroids, comets and moons of planets. According to their results, there are usually four equilibrium points outside the elongated bodies. This is one reason that the rotating mass dipole can be used to approximate elongated bodies. The discussions on equilibrium points undoubtedly benefit the understanding of the topological structure and would be significant for the trajectory designs of space probes in the vicinity of these irregularly shaped bodies.

The focus of this study is the extension of the rotating mass dipole when oblateness is present in both primaries. The equilibrium points of such a system have never been fully investigated. It is also expected that this paper could provide some common properties of equilibrium points around elongated bodies by varying their system parameters. The contents are organized as follows. Section 2 introduces the dynamical equations of the dipole system with oblateness of two primaries. The characteristic equations of equilibria associated with such a system are derived in Section 3, with respect to the equatorial plane and the plane xoz. In Section 4, numerical simulations are performed by considering all three scenarios of the perturbed dipole model, including double oblate, double prolate and oblate-prolate primaries. Finally, the influence of oblateness in the primary on topological structure near the central body is discussed by taking the scenario of oblate-prolate primaries as a representative example.

2 DYNAMIC EQUATIONS OF THE PERTURBED DIPOLE MODEL

The originally proposed dipole model is composed of two point masses which are connected with a massless rod at a constant distance (Chermnykh 1987). Here, the two point masses are replaced by two spheroids m_1 and m_2 with a natural assumption of $m_1 \geq m_2$. They rotate around their common center of mass with an angular velocity of $\boldsymbol{\omega}$ aligned with the principal axis that has the highest moment of inertia. To keep a constant distance d between the two primaries, the massless rod may provide a compressive or tensile force.

Figure 1 illustrates the body-fixed frame $oxyz$ (also known as the synodical frame) for the dipole model where the two primaries can be oblate or prolate spheroids. The origin of $oxyz$ is at the barycenter of the system while its plane oxy coincides with the equatorial plane of the dipole system. The axis ox is collinear with the two primaries pointing from m_1 to m_2. The axis oz is along the direction of angular velocity resulting in $\boldsymbol{\omega} = \omega \boldsymbol{z}$ while axis oy completes the right-handed frame.

When a spacecraft orbits an asteroid with a non-negligible physical size, the spacecraft can be mostly treated as a point mass. The dynamic equations of a par-

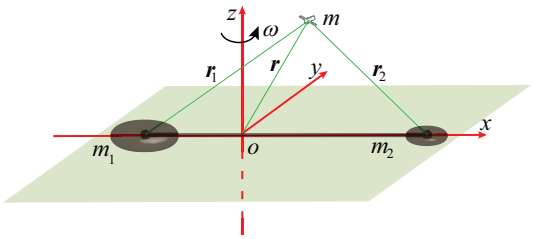

Fig. 1 The body-fixed frame $oxyz$ for the rotating dipole with oblateness in both primaries.

ticle around a minor body can be written in the form

$$\ddot{\boldsymbol{r}} + 2\boldsymbol{\omega} \times \dot{\boldsymbol{r}} + \boldsymbol{\omega} \times (\boldsymbol{\omega} \times \boldsymbol{r}) + \dot{\boldsymbol{\omega}} \times \boldsymbol{r} = -\nabla U, \quad (1)$$

where $\boldsymbol{r}$ is the position vector from the origin to the spacecraft as shown in Figure 1. The right term ∇U is the gradient of the effective potential of the dipole model. Its definition is $U = G \cdot (m_1/r_1 + m_2/r_2)$ where G is the gravitational constant with a value of 6.67×10^{-11} $\mathrm{m^3\,kg^{-1}\,s^{-2}}$. The parameters r_i (i = 1, 2) are the distance between the particle and the primaries, respectively. Since most celestial bodies in the solar system are in a pure spinning state with respect to the principle axis, representing the highest moment of inertia, the term $\dot{\omega}$ can be zero.

To improve the calculation efficiency, dimensionless units are applied to Equation (1). The length unit is set as d, i.e., the distance between the two primaries, the mass unit is the system mass $M = m_1 + m_2$ and the time unit is ω^{-1}. Given the mass ratio $\mu = m_2 / M$, the positions of the two tip masses m_1 and m_2 are $[-\mu, 0, 0]^{\mathrm{T}}$ and $[1-\mu, 0, 0]^{\mathrm{T}}$, respectively. Here, the investigated region of the mass ratio is (0, 0.5] without considering the case of μ = 0. The position vectors of the particle with respect to m_1 and m_2 after the unit transformation are

$$\boldsymbol{r}_1 = [x+\mu, y, z]^{\mathrm{T}}, \boldsymbol{r}_2 = [x+\mu-1, y, z]^{\mathrm{T}}. \quad (2)$$

Since the centrifugal term in Equation (1) is conserved, the dynamic equations can be re-organized as

$$\ddot{\boldsymbol{r}} + 2\boldsymbol{\omega} \times \dot{\boldsymbol{r}} = -\nabla V, \quad (3)$$

where the new effective potential V can be expressed explicitly with

$$V = -\frac{\omega^2}{2} \cdot \left(x^2 + y^2\right) - \kappa\omega^2 \cdot \left(\frac{1-\mu}{r_1} \cdot W_1 + \frac{1-\mu}{r_2} \cdot W_2\right), \quad (4)$$

and the functions W_i are

$$W_i = 1 + \frac{A_i}{2r_i^2} \cdot \left(1 - \frac{3z^2}{r_i^2}\right), \quad i = 1, 2. \quad (5)$$

The dimensionless parameter κ derived in Equation (4) is very important whose definition is

$$\kappa = \frac{GM/d^2}{\omega^2 d} = \frac{GM}{\omega^2 d^3}. \quad (6)$$

One can easily note that it represents the ratio between the gravitational force and the centrifugal force, usually referred to as 'the force ratio.' If the value of κ is exactly unity, then the dipole model will degenerate to the classical circular restricted three body problem (CRTBP) (Szebehely 1967) with oblateness in both primaries. Therefore, the rotating dipole model is a generalization of the CRTBP in terms of the dynamical equations.

The original CRTBP was proposed in the 1770s with applications to the Trojan asteroids (Hou et al. 2014), the Sun-Earth system and similar dynamical systems (Szebehely 1967), while the modified CRTBP with oblateness of primaries can be dated back to the 1970s. Many authors, such as Vidyakin (1974), Sharma & Rao (1976) and Idrisi (2014), have investigated this problem with theoretical discussions. In 2003, Oberti & Vienne (2003) successfully applied this theory to the Saturn system based on observed data, by considering the effect of Saturn's oblateness on the motions of Tethys and Dione's Lagrangian moons Telesto, Calypso and Helene. These studies will undoubtedly be beneficial for the analysis of the dipole problem in this paper.

The dimensionless angular velocity of the perturbed dipole model in Equation (4) is no longer unity. It should be updated with

$$\omega = \sqrt{1 + \frac{3}{2}(A_1 + A_2)}, \quad (7)$$

where A_i (i = 1, 2) is the oblateness coefficient of the primaries, whose definition is (Sharma & Rao 1976)

$$A_i = \frac{\left(\rho_i^{\mathrm{e}}\right)^2 - \left(\rho_i^{\mathrm{p}}\right)^2}{5d^2}, \quad i = 1, 2, \quad (8)$$

where the parameter ρ is the radius of the primary as a spheroid. The superscript 'e' represents the equatorial radius of the primary while 'p' corresponds to its polar radius. Different from the CRTBP, the value of A_i (i = 1, 2) can be negative for the perturbed dipole model corresponding to a prolate spheroid.

Substituting Equation (4) and Equation (5) into Equation (3) yields the scalar form of the dynamic equations

$$\left[\ddot{x}, \ddot{y}, \ddot{z}\right]^{\mathrm{T}} + [-2\omega\dot{y}, 2\omega\dot{x}, 0]^{\mathrm{T}} = -\left[\nabla V_x, \nabla V_y, \nabla V_z\right]^{\mathrm{T}}, \quad (9)$$

where the gradients of the effective potential are specified as

$$\nabla V_x = -\omega^2 \cdot \Big\{ x - \kappa \cdot \Big[\frac{(1-\mu)(x+\mu)}{r_1^3} \cdot Q_1 + \frac{\mu(x+\mu-1)}{r_2^3} \cdot Q_2 \Big] \Big\}, \tag{10}$$

$$\nabla V_y = -\omega^2 y \cdot \left[1 - \kappa \cdot \left(\frac{1-\mu}{r_1^3} \cdot Q_1 + \frac{\mu}{r_2^3} \cdot Q_2 \right) \right], \tag{11}$$

$$\nabla V_z = \kappa\omega^2 z \cdot \left[\frac{1-\mu}{r_1^3} \cdot \left(Q_1 + \frac{3A_1}{r_1^2} \right) + \frac{\mu}{r_2^3} \cdot \left(Q_2 + \frac{3A_2}{r_2^2} \right) \right], \tag{12}$$

and the auxiliary function Q is defined as

$$Q_i = 1 + \frac{3A_i}{2r_i^2} - \frac{15A_i z^2}{2r_i^4}, \quad i = 1,\, 2, \tag{13}$$

and the subscript 'i' corresponds to the two primaries.

The dynamic system of Equation (9) in the synodic coordinate frame leads to the Jacobi's integral

$$C = \frac{\dot{\boldsymbol{r}}\dot{\boldsymbol{r}}}{2} + V, \tag{14}$$

which is the only conserved term found for such a dynamical system up until now. The case of $C = V$ in Equation (14) specifies a surface in the configuration space, usually termed the zero-velocity surface, determining the allowable region of the possible motion for a particle in the vicinity.

3 EQUILIBRIUM POINTS OF THE DIPOLE SYSTEM

The equilibrium points of the perturbed dipole system can be categorized into two groups. One is in the equatorial plane and the other is out of plane, specifically, located in the plane xoz perpendicular to the equatorial plane. Similar to the CRTBP, there should be some collinear equilibrium points and some Lagrange points (also non-collinear equilibrium points). The equilibria of the dipole system can be obtained with zero values of both velocities and accelerations in Equation (9) corresponding to the right terms also being zero

$$[\nabla V_x,\, \nabla V_y,\, \nabla V_z]^{\mathrm{T}} = \mathbf{0}. \tag{15}$$

Based on the above equation, the positions of collinear equilibrium points will be first derived, followed by the non-collinear equilibria and out-of-plane equilibrium points.

3.1 Equilibrium Points in the Equatorial Plane

For equilibrium points in the equatorial plane, the value of z is zero, resulting in the third component of Equation (15), ∇V_z, being zero. Therefore, the positions of the equilibria can be located by setting both Equation (10) and Equation (11) to zero as

$$x - \kappa \cdot \left[\frac{(1-\mu)\,(x+\mu)}{r_1^3} \cdot Q_1 + \frac{\mu\,(x+\mu-1)}{r_2^3} \cdot Q_2 \right] = 0, \tag{16}$$

and

$$y \cdot \left[1 - \kappa \cdot \left(\frac{1-\mu}{r_1^3} \cdot Q_1 + \frac{\mu}{r_2^3} \cdot Q_2 \right) \right] = 0, \tag{17}$$

where the angular velocity of the dipole system is always positive. The collinear equilibrium points can be obtained by setting y = 0 in Equation (17) satisfying the condition

$$x - \kappa \cdot \left[\frac{(1-\mu)\,(x+\mu)}{|\, x+\mu\,|^3} \cdot \left(1 + \frac{3A_1}{2\,|\, x+\mu\,|^2} \right) + \frac{\mu\,(x+\mu-1)}{|\, x+\mu-1\,|^3} \cdot \left(1 + \frac{3A_2}{2\,|\, x+\mu-1\,|^2} \right) \right] = 0. \tag{18}$$

With the definition of two auxiliary sign functions

$$\begin{aligned} s_1 &= \mathrm{sign}\,(x+\mu)\,, \\ s_2 &= \mathrm{sign}\,(x+\mu-1)\,, \end{aligned} \tag{19}$$

one can rewrite Equation (18) without the absolute values as

$$x - \kappa \cdot \left[\frac{(1-\mu)\cdot s_1}{(x+\mu)^2} \cdot \Big(1 + \frac{3A_1}{2(x+\mu)^2} \Big) + \frac{\mu \cdot s_2}{\big(x+\mu-1\big)^2} \cdot \Big(1 + \frac{3A_2}{2\big(x+\mu-1\big)^2} \Big) \right] = 0, \tag{20}$$

yielding a nonlinear equation of x in the form of a polynomial. The nonlinear equation with the highest degree of nine will be directly solved by the *Matlab* function '*fsolve*' with a tolerance of 10^{-10} to guarantee the accuracy of the collinear equilibrium points.

For the non-collinear equilibria in the equatorial plane with $y \neq 0$, Equation (17) would be satisfied with

$$1 - \kappa \cdot \left(\frac{1-\mu}{r_1^3} \cdot Q_1 + \frac{\mu}{r_2^3} \cdot Q_2 \right) = 0. \tag{21}$$

Combining the above equation with Equation (16) gives

$$2r_i^5 - 2\kappa r_i^2 - 2\kappa A_i = 0, \quad i = 1,\, 2. \tag{22}$$

Equation (22) indicates that the distance between the non-collinear equilibrium point and the primary must satisfy the above quantic polynomial. Hence, the non-collinear equilibrium point is the intersection point of two circles. One circle is centered at m_1 with a radius of r_1 and the other is centered at m_2 with a radius of r_2. Meanwhile, the magnitude of the radius, i.e., r_1 and r_2, only depends on the force ratio and the oblateness coefficient. Note that there may be two positive roots of Equation (22) for the case of a negative oblateness coefficient, indicating that new non-collinear equilibria will be found for such a system compared to the CRTBP.

By solving the above equation, the radii r_1 and r_2 can be obtained. Combining with Equation (2), the coordinate values x of the non-collinear equilibria can be calculated

$$x_{\rm T} = \frac{r_1^2 - r_2^2}{2} + \frac{1}{2} - \mu, \tag{23}$$

where the subscript 'T' denotes the non-collinear points. Their corresponding y-coordinates should be

$$\begin{aligned} y_{\rm T} &= \pm\sqrt{r_1^2 - (x_{\rm T}+\mu)^2} \\ &= \pm\sqrt{r_2^2 - (x_{\rm T}+\mu-1)^2}, \end{aligned} \tag{24}$$

which indicates there is always a pair of non-collinear equilibria axisymmetric with respect to the axis ox except for the boundary case of a double root.

3.2 Out-of-Plane Equilibrium Points

The discovery of out-of-plane equilibrium points may have been first made by Radzievskii (1950) for a Sun-planet-particle system, where two additional equilibrium points in the xoz plane were found. Such equilibria were also found by Ragos & Zagouras (1993) in the photo-gravitational restricted three body problem. Douskos & Markellos (2006) analyzed the existence of such equilibrium points in the CRTBP by considering the oblateness of the less massive primary. In this paper, such investigations will be extended to the case of both primaries having oblateness.

As seen from Equation (15) and Equations (10)–(12), the positions of the out-of-plane equilibrium points with $y = 0$ and $z \neq 0$ should fulfill Equation (16) and the remaining equation

$$\frac{1-\mu}{r_1^3}\cdot\left(Q_1 + \frac{3A_1}{r_1^2}\right) + \frac{\mu}{r_2^3}\cdot\left(Q_2 + \frac{3A_2}{r_2^2}\right) = 0. \tag{25}$$

It seems impossible to obtain analytical solutions of Equation (16) and Equation (25). Hence, approximate solutions in the form of power series to third order are usually generated by using the software *Mathematica*. Here, the locations of these equilibria will be found via numerical simulations in the next section.

4 NUMERICAL EXAMPLES AND DISCUSSIONS

The distribution of equilibrium points for the perturbed dipole system will be given via numerical simulations. Only a few sample cases will be presented and parametric studies will be neglected in this section. For example, the parameters of the dipole model in the following discussions are arbitrarily set to be κ = 1 and μ = 0.5. Different values of κ and μ correspond to different gravitational potential distributions which can be seen from the result of Zeng et al. (2015a). The boundary condition for the oblate primary should be a circular disk while a massive straight segment centered at the prolate primary along the axis oz is the other limiting case. For the above two boundary conditions, the respective values of the oblateness coefficient are 0.05 and -0.05, which will be used in the subsequent simulations.

4.1 Case of Double Oblate Primaries

Figure 2 illustrates the locations of equilibrium points in the equatorial plane oxy along with the zero-velocity curves. The oblateness coefficients for both primaries are 0.05. The five equilibria are similar to the classical Lagrange points L_1 to L_5, i.e., four exterior points E_2 to E_5 and one inner point E_1. The coordinates of these points are listed in Table 1. For this particular case, the gravitational potential of the rotating mass dipole is symmetrical with respect to all three planes, including xoy, xoz and yoz. If both primaries are supposed to be point masses, then the perturbed dipole model will degenerate into the classical dipole model. For the classical dipole model, the coordinates of its equilibria can be obtained as $x\,(E_2) = 1.1984$, $y\,(E_2) = 0$, $x(E_4) = x(E_5) = 0$ and $y(E_4) = -y(E_5) = 0.8660$. Thus, it can be found that all exterior equilibria move far away from the oblate primaries.

For each oblate primary, there is also a pair of equilibrium points nearly right above and below the oblate spheroid. Such a case has been analyzed by Zeng et al. (2016a). To assure the integrity of this paper, it will be also briefly discussed. These points are shown in Figure 3 along with zero-velocity curves in the plane xoz and their coordinates are listed in Table 1. Note that these points are obtained by solving the nonlinear equations of Equation (16) and Equation (25). Based on the research work done by Douskos & Markellos (2006), the initial values of $x_0 = 1 - \mu$ and $z_0 = \sqrt{3|A_2|}$ are effective for obtaining the equilibria E_{z1} and E_{z2} near m_2. Similarly,

Table 1 Positions of Equilibrium points of the Dipole Model with Double Oblate Primaries

	E_1	E_2	E_3	E_4	E_5	E_{z1}	E_{z2}	E_{z3}	E_{z4}
x	0	1.235	–1.235	0	0	0.493	0.493	–0.493	–0.493
y	0	0	0	0.893	–0.893	0	0	0	0
z	0	0	0	0	0	0.377	–0.377	0.377	–0.377

Table 2 Positions of Equilibrium Points of the Dipole Model with Double Prolate Primaries

	E_1	E_2	E_3	E_4	E_5	L_{N1}	L_{N2}	L_{N3}	L_{N4}
x	0	1.151	–1.151	0	0	0.210	0.786	0.435	0.435
y	0	0	0	0.835	–0.835	0	0	0.269	–0.269

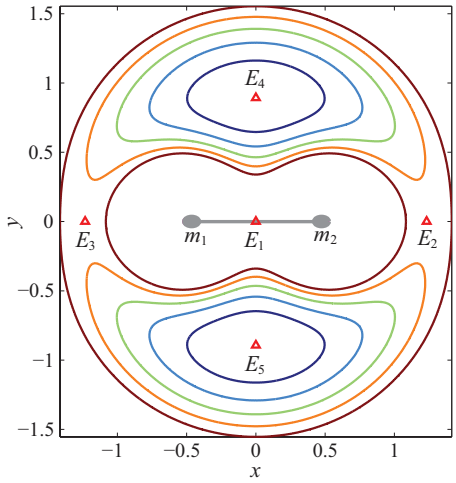

Fig. 2 Equilibria in the equatorial plane and zero-velocity curves for the rotating mass dipole with two oblate primaries.

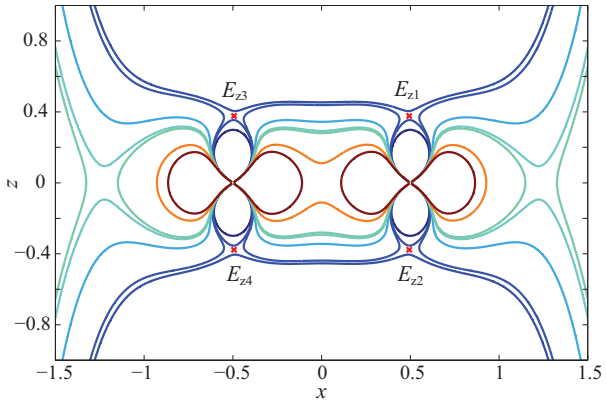

Fig. 3 Equilibrium points in the plane xoz and zero-velocity curves for the dipole model with two oblate primaries.

the initial values of $x_0 = -\mu$ and $z_0 = \sqrt{3|A_1|}$ are used to determine the equilibria E_{z3} and E_{z4} around m_1.

4.2 Case of Double Prolate Primaries

From Figure 2, the topological structure in the plane xoy of the perturbed dipole system with double oblate primaries is similar to that of the CRTBP with minor changes. However, for the dipole model with double prolate primaries, the topological structure in the plane xoy given in Figure 4 is totally different from that of the CRTBP. The oblateness coefficients for the two prolate primaries are -0.05. To clearly show the new equilibria, Figure 4(a) presents the distribution of equilibria in the plane xoy marked with their corresponding names. In Figure 4(b), zero-velocity curves are illustrated to show the topological structure around the dipole model along with the equilibrium points.

There are a total of 13 equilibrium points in the plane xoy. Due to the prolate primary, four additional equilibria L_{N1} to L_{N4} near m_2 are found whose coordinates are listed in Table 2. Around the primary m_1, another four equilibria L_{N5} to L_{N8} are also found which are symmetrical with L_{N1} to L_{N4} with respect to the axis oy. For example, it satisfies $x(L_{N(i+4)}) = -x(L_{Ni})$ and $y(L_{N(i+4)}) = y(L_{Ni})$ where i = 1, 2, 3, 4. Therefore, the coordinates of L_{N5} to L_{N8} are not given in Table 2. It should be pointed out that the symmetrical property about axis oy is only fulfilled with $A_1 = A_2$. If the oblateness coefficients of the two primaries are different, the symmetrical property with respect to axis oy will be invalid. Particularly, the exterior points E_2 to E_4 move close to the prolate primaries based on Table 2.

For the above case, no equilibrium point is found in the plane xoz. Hence, the emergence of out-of-plane equilibria is due to the oblate spheroid while the prolate spheroid can produce new equilibria in the equatorial plane. The influence of the system parameters on the equilibrium points has been addressed by Zeng et al. (2015a, 2016a), including the oblateness coefficient, the force ratio and the mass ratio by only considering the oblateness of the second primary. Such parametric studies will be neglected in consideration of the length of this paper.

It should be stated that the oblateness coefficient of 0.05 or -0.05 may be relatively too large to find corresponding physical minor celestial bodies. In general, the oblateness coefficient for the restricted three body problem is at the level of 10^{-3}. For example, the maximum value is approximately 0.004 for the Saturn-Mimas

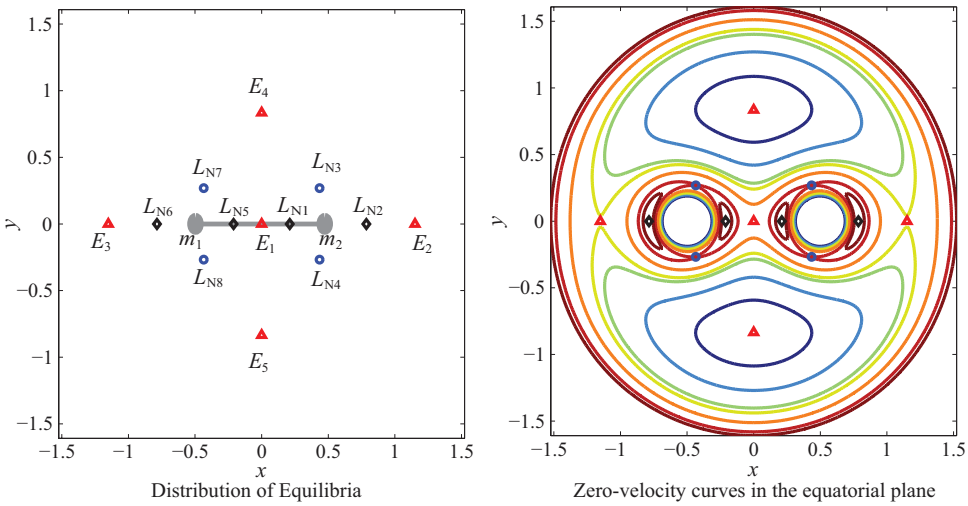

Fig. 4 Equilibrium points in the equatorial plane and zero-velocity curves for the rotating mass dipole with both primaries being prolate.

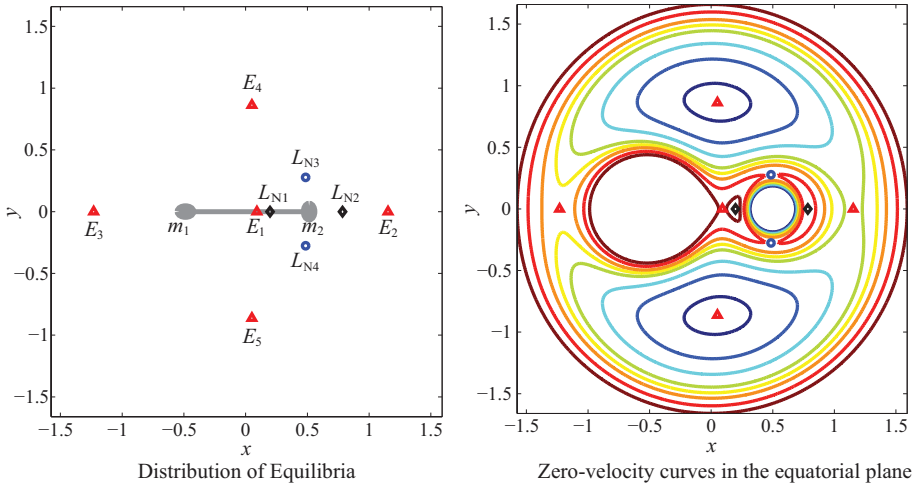

Fig. 5 Equilibrium points in the equatorial plane and zero-velocity curves for the rotating mass dipole with oblate-prolate primaries.

system (Sharma & Rao 1976). As for elongated asteroids with small values of oblateness coefficients, the new equilibria L_N and E_z should be very near the oblate or prolate primaries which are expected at the inner part of the central body. That is also the reason why we call E_2 to E_5 exterior equilibrium points.

4.3 Case of Oblate-Prolate Primaries

From Sections 4.1 and 4.2, it can be estimated that for the case of the dipole model with oblate-prolate primaries, there should be a total of 11 equilibrium points, i.e., nine points in the plane xoy and two in the plane xoz.

Figure 5 shows the locations of the equilibrium points in the plane xoy along with zero-velocity curves. The example here fully represents the case of one oblate primary and one prolate primary since the first primary can be prolate by rotating the model by 180 degrees. Figure 6 illustrates the out-of-plane equilibria around the prolate spheroid m_2 and zero-velocity curves.

With oblate-prolate primaries, the gravitational potential of the dipole model still maintains the symmetrical property with respect to the plane xoz and xoy. It has been pointed out that the exterior equilibria E_2 to E_5 get shifted away from oblate primaries while prolate primaries attract these points to approach themselves. For this particular case, the point E_1 is not at the origin whose value is 0.091 as seen from Table 3 where all of the equilibrium points in the system have been listed. Such a result is also consistent with the analysis that the

Table 3 Positions of Equilibrium Points of the Dipole Model with Oblate-Prolate Primaries

	E_1	E_2	E_3	E_4	E_5	L_{N1}	L_{N2}	L_{N3}	L_{N4}	E_{z1}	E_{z2}
x	0.091	1.153	–1.231	0.050	0.050	0.197	0.785	0.485	0.485	0.491	0.491
y	0	0	0	0.863	–0.863	0	0	0.276	–0.276	0	0
z	0	0	0	0	0	0	0	0	0	0.38	–0.38

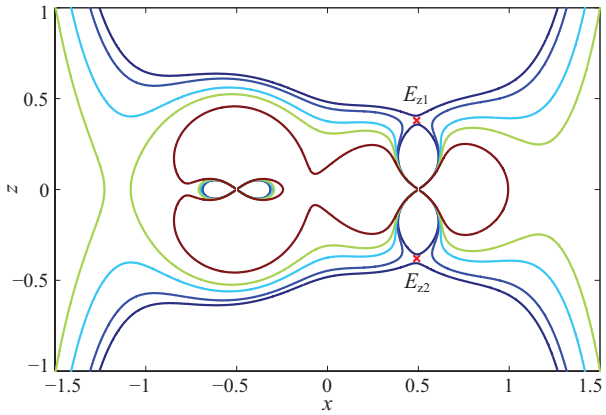

Fig. 6 Equilibrium points in the plane xoz and zero-velocity curves for the dipole model with oblate-prolate primaries.

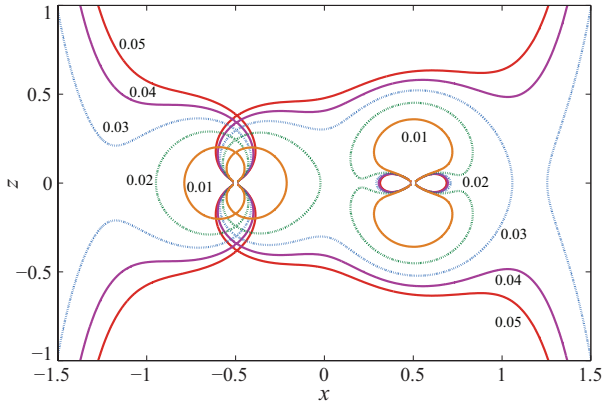

Fig. 7 Influence of the first oblate primary A_1 on zero-velocity curves in the plane xoz.

equilibria move away from the oblate primary and approach the prolate primary. However, such rules cannot be applied to the new equilibrium points.

Above all, all three cases of the dipole model with oblateness in both primaries have been presented via numerical examples to fully introduce the attributes of the equilibrium points. The simulation conditions are specified as $[\kappa,\ \mu,\ |A_i|]^{\mathrm{T}} = [1, 0.5, 0.05]$ where $i = 1, 2$. Besides the five classical equilibria associated with the CRTBP, new equilibrium points are obtained due to the oblateness of the primaries. For each prolate primary, there could be four additional equilibria in the equatorial plane. While for the oblate primary, a pair of out-of-plane equilibria can be found in the plane xoz. The maximum number of equilibrium points for the proposed dipole system is 13 corresponding to the case of two prolate primaries.

The stability of the system equilibria is a significant problem for understanding the dynamical behaviors around these points. The method used by Zeng et al. (2015a) could be adopted to investigate the stability of these points. Based on the results given by Zeng et al. (2015a, 2016a), it can be predicted that the equilibria E_1 (Hirabayashi et al. 2010), E_4, E_5, L_{N1}, L_{N2}, L_{N5} and L_{N6} are conditionally stable, dependent on the values of $[\kappa,\ \mu,\ |A_i|]^{\mathrm{T}}$ (i = 1, 2). Other equilibrium points, including E_2, E_3, L_{N3}, L_{N4}, L_{N7}, L_{N8} and E_{zi} (i = 1, 2, 3, 4), should be expected to be unstable. Due to the length of this paper, the stability of these equilibrium points will be left for further investigations.

5 INFLUENCE OF OBLATENESS ON TOPOLOGICAL STRUCTURES

The oblateness of the primary plays an important role in the topological structure around the dipole system. In this section such an effect will be investigated through checking the variation of the zero-velocity surface by varying the oblateness coefficient. The system parameters are $[\kappa,\ \mu,\ |A_2|]^{\mathrm{T}}$ =$[1,\ 0.5,\ -0.05]^{\mathrm{T}}$ which are representative of the perturbed dipole model. The investigated region for the variable A_1 is $[-0.05,\ 0.05]$. For the case of positive A_1, zero-velocity curves, in the plane xoz in the values of Jacobi's integral corresponding to the out-of-plane equilibrium points E_{z3} (E_{z4}), are shown in Figure 7. For clarity, the sketch map of the dipole model is not illustrated in the figure. The topological structure changes a lot along with the increase of A_1 from 0.01 to 0.05.

The projection of the zero-velocity surface in the plane xoy is given in Figure 8 with four independent figures corresponding to different values of A_1. The curves in each figure correspond to the Jacobi integral's values of E_3, E_4, L_{N7} (L_{N8}) and L_{N1}. Along with the increase A_1 from –0.05 to –0.01, noticeable changes in the zero-velocity curves can be found at the region between m_1 and m_2, transforming from the forbidden area to the nearly connected region. Such variations should be considered for the motion of surrounding particles very close to the dipole model.

Besides the above theoretical discussions on the improved dipole model, additional comments are made to

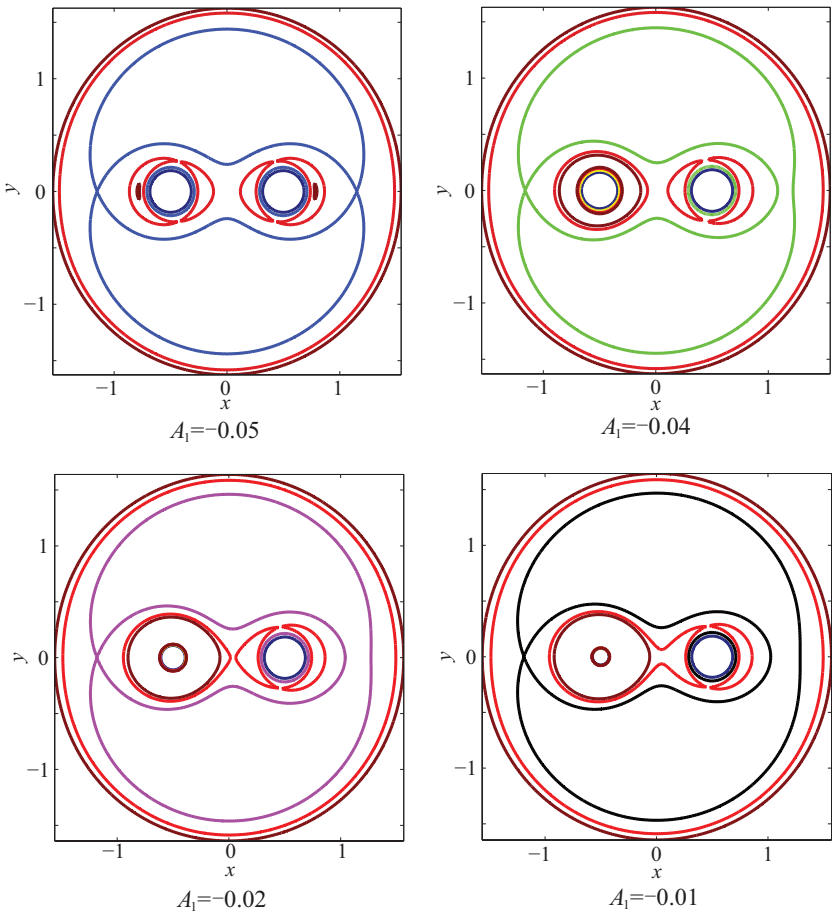

Fig. 8 Influence of the first prolate primary on zero-velocity curves in the plane xoy.

introduce potential applications of this model. Although the dipole model can reduce the calculation effort and simplify the gravitational function, it is only a rough approximation for real asteroids. Even if the asteroid can be nearly treated as two connected spheroids, they may not be aligned along their symmetry axes. Nevertheless, it can also be approximated by using the dipole model, because we recently found that the dipole model can be treated as a special case of the mass concentration approach, usually referred to as Mascons (Colagrossi et al. 2015). The improved model including oblateness is expected to be more accurate to some extent in depicting dumbbell-shaped asteroids.

Another application of the above model is to approximate the potential distribution of doubly synchronous binary asteroid systems (Shang et al. 2015), where the force ratio is always unity. As a preliminary estimation, the CRTBP with a corresponding mass ratio will be worked out. Due to the close distance of the two bodies, it would be better to take the oblateness of the primaries into account, in which the improved dipole model degenerates to the model of Sharma & Rao (1976). Moreover, the zonal and tesseral terms in higher orders of the primaries, such as C22, C30 and C31, should be considered for different asteroids, which may be comparable with the C20 term (Feng et al. 2015). Such a problem should not be overlooked, particularly in the near realm of asteroids, which will be left for further studies.

6 CONCLUDING REMARKS

An improved dipole model has been proposed by considering the oblateness of both primaries. Besides the five equilibrium points in the equatorial plane similar to the classical Lagrange points of the CRTBP, new equilibria were obtained due to the oblateness of the primaries. A total of three topological scenarios have been analyzed including the double oblate, double prolate and oblate-prolate spheroids. For an oblate primary with a positive oblateness coefficient, a pair of new equilibrium points in the plane oxz was found located nearly right above and below its polar regions. For the case of a negative

coefficient, four new equilibria have been discovered in the equatorial plane near the prolate primary. There are up to 13 equilibrium points for the case of double prolate primaries.

The significant influence of the primary's oblateness on the topological structure around the dipole model has been presented by using the zero-velocity curves in both planes oxy and oxz. With the increase of the oblateness coefficient, the forbidden region of motion near the dipole model in the same Jacobi's integral gradually opened up to be unified with previously allowable areas for the oblate primary in the plane oxz. By varying the oblateness coefficient, zero-velocity curves in the near region of the dipole model change a lot from separated regions to a unified area. The above discussions would benefit the understanding of the dynamic environment close to elongated asteroids and binary asteroid systems.

Acknowledgements This work was supported by the National Natural Science Foundation of China (Nos. 11602019 and 11572035) and China Postdoctoral Science Foundation (2015T80077). The Excellent Young Teachers Program of Beijing Institute of Technology and Beijing Institute of Technology Research Fund Program for Young Scholars are also acknowledged. The comments on applications of the model in this paper from anonymous reviewer(s) are appreciated.

References

Bartczak, P., & Breiter, S. 2003, Celestial Mechanics and Dynamical Astronomy, 86, 131

Chermnykh, S. V. 1987, Leningradskii Universitet Vestnik Matematika Mekhanika Astronomiia, 1, 73

Colagrossi, A., Ferrari, F., Lavagna, M., & Howell, K. 2015, in AAS/AIAA Conference, no. AAS, 15

Cui, P., & Qiao, D. 2014, Theoretical and Applied Mechanics Letters, 4, 013013

Douskos, C. N., & Markellos, V. V. 2006, A&A, 446, 357

Elipe, A., Lara, M. 2003, JAS, 51, 391 *http://www.unizar.es/galdeano/preprints/2004/preprint06.pdf*

Feng, J., Noomen, R., Visser, P. N. A. M., & Yuan, J. 2015, Ap&SS, 357, 124

Fountain, G. H., Kusnierkiewicz, D. Y., Hersman, C. B., et al. 2008, Space Sci. Rev., 140, 23

Gong, S., Li, J., & Baoyin, H. 2009, Celestial Mechanics and Dynamical Astronomy, 105, 159

Goździewski, K. 1998, Celestial Mechanics and Dynamical Astronomy, 70, 41

Hirabayashi, M., Morimoto, M. Y., Yano, H., Kawaguchi, J., & Bellerose, J. 2010, Icarus, 206, 780

Hou, X. Y., Scheeres, D. J., & Liu, L. 2014, MNRAS, 437, 1420

Huang, J., Ji, J., Ye, P., et al. 2013, Scientific Reports, 3, 3411

Idrisi, M. J. 2014, Ap&SS, 354, 311

Jiang, Y., Ji, J., Huang, J., et al. 2015, Scientific Reports, 5, 16029

Kokoriev, A., & Kirpichnikov, S. 1988, Vestn. Leningr. Univ, 1, 75

Li, X., Qiao, D., & Cui, P. 2013, Ap&SS, 348, 417

Magri, C., Howell, E. S., Nolan, M. C., et al. 2011, Icarus, 214, 210

Mondelo, J.-M., Broschart, S. B., & Villac, B. F. 2010, in Proceedings of the 2010 AIAA/AAS Astrodynamics Specialists Conference, Aug, 2

Oberti, P., & Vienne, A. 2003, A&A, 397, 353

Ostro, S. J., Hudson, R. S., Nolan, M. C., et al. 2000, Science, 288, 836

Prieto-Llanos, T., & Gomez-Tierno, M. A. 1994, Journal of Guidance Control Dynamics, 17, 787

Radzievskii, V. V. 1950, Astron. Ž, 27, 250 (in Russian)

Ragos, O., & Zagouras, C. G. 1993, Ap&SS, 209, 267

Scheeres, D. J., Ostro, S. J., Hudson, R. S., DeJong, E. M., & Suzuki, S. 1998, Icarus, 132, 53

Scheeres, D. J. 2014, Nature, 512, 139

Shang, H., Wu, X., & Cui, P. 2015, Ap&SS, 355, 69

Sharma, R. K., & Rao, P. S. 1976, Celestial Mechanics, 13, 137

Szebehely, V. 1967, Theory of orbits. The Restricted Problem of Three Bodies (New York: Academic Press)

Tsuchiyama, A., Uesugi, M., Matsushima, T., et al. 2011, Science, 333, 1125

Vidyakin, V. 1974, Astron. Zh, 51, 1087

Wang, X., Jiang, Y., & Gong, S. 2014, Ap&SS, 353, 105

Werner, R. A., & Scheeres, D. J. 1996, Celestial Mechanics and Dynamical Astronomy, 65, 313

Yang, H., Gong, S., & Baoyin, H. 2015, Astrophysics and Space Science, 357, 66

Zeng, X., Jiang, F., Li, J., & Baoyin, H. 2015a, Ap&SS, 356, 29

Zeng, X.-Y., Jiang, F.-H., & Li, J.-F. 2015b, RAA (Research in Astronomy and Astrophysics), 15, 597

Zeng, X., Baoyin, H., & Li, J. 2016a, Ap&SS, 361, 15

Zeng, X., Gong, S., Li, J., & Alfriend, K. T. 2016b, Journal of Guidance Control Dynamics, 39, 1223

Zhao, Y., Ji, J., Huang, J., et al. 2015, MNRAS, 450, 3620

Zou, X., Li, C., Liu, J., et al. 2014, Icarus, 229, 348